Surface chemical heterogeneity modulates silica surface hydration

Alex M. Schrader[a], Jacob I. Monroe[a], Ryan Sheil[b], Howard A. Dobbs[a], Timothy J. Keller[c], Yuanxin Li[c], Sheetal Jain[c], M. Scott Shell[a], Jacob N. Israelachvili[a,d,1], and Songi Han[a,c]

[a]Department of Chemical Engineering, University of California, Santa Barbara, CA 93106-5080; [b]Department of Chemical and Biomolecular Engineering, University of California, Los Angeles, CA 90095-1592; [c]Department of Chemistry and Biochemistry, University of California, Santa Barbara, CA 93106-5050; and [d]Materials Department, University of California, Santa Barbara, CA 93106-5050

Contributed by Jacob N. Israelachvili, February 8, 2018 (sent for review December 21, 2017; reviewed by Paul S. Cremer and Peter J. Rossky)

An in-depth knowledge of the interaction of water with amorphous silica is critical to fundamental studies of interfacial hydration water, as well as to industrial processes such as catalysis, nanofabrication, and chromatography. Silica has a tunable surface comprising hydrophilic silanol groups and moderately hydrophobic siloxane groups that can be interchanged through thermal and chemical treatments. Despite extensive studies of silica surfaces, the influence of surface hydrophilicity and chemical topology on the molecular properties of interfacial water is not well understood. In this work, we controllably altered the surface silanol density, and measured surface water diffusivity using Overhauser dynamic nuclear polarization (ODNP) and complementary silica–silica interaction forces across water using a surface forces apparatus (SFA). The results show that increased silanol density generally leads to slower water diffusivity and stronger silica–silica repulsion at short aqueous separations (less than ∼4 nm). Both techniques show sharp changes in hydration properties at intermediate silanol densities (2.0–2.9 nm^{-2}). Molecular dynamics simulations of model silica–water interfaces corroborate the increase in water diffusivity with silanol density, and furthermore show that even on a smooth and crystalline surface at a fixed silanol density, adjusting the spatial distribution of silanols results in a range of surface water diffusivities spanning ∼10%. We speculate that a critical silanol cluster size or connectivity parameter could explain the sharp transition in our results, and can modulate wettability, colloidal interactions, and surface reactions, and thus is a phenomenon worth further investigation on silica and chemically heterogeneous surfaces.

water | silica | hydration dynamics | surface forces | hydrophobicity

Silicon dioxide, SiO_2, or glass, is a ubiquitous material particularly relevant to catalysis, geology, and semiconductor processing (1). Despite the immense literature on the properties of SiO_2 surfaces, the molecular details of the SiO_2–water interface—specifically, the exact chemical makeup of the surface as a function of pretreatment conditions, and the resulting impact on the hydrophilicity and hydration barrier of the surface—are not well understood. It is accepted that the SiO_2 surface comprises silanol (SiOH) groups that are hydrophilic, and siloxane (SiOSi) groups that are moderately hydrophobic (1, 2), but any general and unifying model of the SiO_2–water interface is lacking, likely due to the existence of SiO_2 of different morphologies (amorphous, crystalline), polymorphism (e.g., quartz, stishovite, cristobalite, coesite), porosity, surface chemistry, and degrees of contamination, which depend on synthesis conditions, preparation methods (e.g., fused, fumed, Stöber/sol–gel, nanofabrication methods), and surface cleaning procedures. Here, we present experimental measurements of the surface forces and surface water diffusivity of nonporous, amorphous silica as a function of surface hydrophilicity (or silanol coverage), accompanied by molecular dynamics simulations that offer molecular insights into the factors that tune surface water diffusivity of mixed hydrophobic/hydrophilic silica surfaces.

The fraction of silanol and siloxane groups on the silica surface is easily adjusted. Under wet or humid conditions, and at equilibrium, the silica surface fully comprises silanol groups (2). When heated above 200 °C, adjacent silanol groups begin to condense to form siloxane bridges via a process known as dehydroxylation. The equilibrium density of silanols on the surface, α_{OH}, has been studied extensively under dry conditions, using techniques such as thermogravimetric analysis (3), infrared spectroscopy (4–7), deuterium exchange (5, 8), ^{29}Si and ^{1}H NMR (3, 6, 9), and titration (10), among others (11). Generally, α_{OH} decreases steadily from ∼4.6 SiOH/nm^2 at temperatures <200 °C, to <0.5 SiOH/nm^2 at ∼1,000 °C (2). Although studies have often disagreed on the true maximum surface silanol density, the disagreement is largely due to the distinction between accessible (surface) or inaccessible (subsurface) silanols (4, 6, 12). Regardless of any quantitative discrepancies, the qualitative trend of decreasing silanol density with temperature is accepted. Siloxane bridges react with water to regenerate silanol groups, a process known as rehydroxylation, but this process can be very slow. Silica surfaces pretreated at 400 °C may fully rehydroxylate within an hour when exposed to liquid water (13, 14), whereas surfaces pretreated at 1,000 °C may take years (1, 2). Additionally, plasma or UV-ozone treatment can rapidly rehydroxylate the surface (15, 16).

Beyond the average silanol density α_{OH}, attempts have also been made to characterize the distribution and coordination of silanol groups, but a complete picture of the surface remains elusive. A combination of infrared spectroscopy (IR), deuterium exchange, and NMR studies has quantified the fraction of vicinal

Significance

Silica, conventionally known as "glass," is a universally used material in catalysis, nanofabrication, and many other applications, but details of its surface chemistry and interactions with water are notoriously complicated and unclear—partially due to its tunable surface chemistry. We utilize this tunable surface chemistry of silica to reveal properties of surface-bound water that impact surface reactions, adhesion, and colloidal interactions. Using a combination of surface forces, hydration dynamics, and simulation techniques, we show that surface silanol groups stabilize the surface water layer, and also that variations/fluctuations are more pronounced at intermediate silanol densities on the surface. This work provides insight into fundamental interactions of water with chemically heterogeneous surfaces.

Author contributions: A.M.S., J.I.M., R.S., M.S.S., J.N.I., and S.H. designed research; A.M.S., J.I.M., R.S., H.A.D., T.J.K., Y.L., and S.J. performed research; A.M.S., J.I.M., R.S., H.A.D., T.J.K., Y.L., S.J., M.S.S., and S.H. contributed new reagents/analytic tools; A.M.S., J.I.M., R.S., T.J.K., Y.L., S.J., M.S.S., J.N.I., and S.H. analyzed data; and A.M.S., J.I.M., M.S.S., J.N.I., and S.H. wrote the paper.

Reviewers: P.S.C., Pennsylvania State University; and P.J.R., Rice University.

The authors declare no conflict of interest.

[1]To whom correspondence should be addressed. Email: jacob@engineering.ucsb.edu.

This article contains supporting information online at www.pnas.org/lookup/suppl/doi:10.1073/pnas.1722263115/-/DCSupplemental.

Published online March 5, 2018.

[Q_3, Si(OH)-O-Si(OH], geminal [Q_2, $Si(OH)_2$], and isolated [Q_3, SiO-Si(OH)-OSi] silanols on the surface as a function of pretreatment temperature (2, 17), or alternatively, the fraction of hydrogen-bonded (proximal) and non–hydrogen-bonded silanols (7, 12, 18). IR measurements of partially dehydroxylated silica in water vapor have shown (somewhat expectedly) that water preferentially adsorbs onto the silanol groups, rather than onto the siloxane bridges (1, 14). Because water is required for rehydroxylation, this result suggests that siloxane bridges adjacent to silanols are more readily hydroxylated than siloxanes distant to silanols. It follows that the growth of silanols is more likely to occur in patches (i.e., autocatalytically) than homogeneously. Recent measurements of the adsorption of $Ga(CH_3)_3$ dimers onto two adjacent silanol groups have shown the potential of quantifying such clustering/coordination experimentally by chemical tools (19). Molecular dynamics simulations of amorphous silica surfaces, while allowing one to clearly visualize the silanol speciation at the surface, have only rarely explored the thermodynamically favorable positioning of silanol groups (20, 21). Rather, most simulation efforts have considered predetermined, fixed chemistries or those constructed via heuristics from bulk, annealed silica (22, 23).

The hydrophilicity of silanol groups arises from their ability to both accept and donate hydrogen bonds (17), whereas siloxane bridges only weakly accept hydrogen bonds (24). However, only a few measurements have experimentally quantified the surface hydrophilicity as a function of α_{OH}. Macroscopic observations of the hydrophilicity of the SiO_2 surface are most clearly seen with water contact angle measurements, where the contact angle (averaged between advancing and receding angles) is <5° on a fully hydroxylated surface, and 40° on an almost fully dehydroxylated surface pretreated at 1,000 °C (25). Force measurements between silica surfaces in water using the surface forces apparatus (SFA) have shown that fully hydroxylated surfaces repel each other strongly below ∼4-nm separation (26–28). Vigil et al. (26) found that dehydroxylated surfaces exhibit a smaller repulsion. However, no systematic study of the silica–silica repulsive forces across water as a function of silanol density has been conducted with the SFA. Vigil et al. proposed that the added short-range repulsion between the hydroxylated surfaces was most likely a steric effect due to protrusion of polysilicic acid groups (or "hairs"), but acknowledged that the results were dependent on the detailed surface preparation method, even for a fixed silanol density. However, SFA measurements by Grabbe showed that coating the silica with an amine monolayer greatly reduced the short-range repulsion (27, 29), which the author(s) used to support the existence of a hydration repulsion, rather than a steric repulsion. Regardless of the differences in interpretation, the contact angle and SFA results alone do not offer conclusive insight into the chemical structure/makeup of the surfaces or the molecular behavior of water at the interface.

In this work, we controllably alter the surface silanol density of silica surfaces α_{OH} through heat treatment, and subsequently use Overhauser dynamic nuclear polarization (ODNP) to measure surface water diffusivity, the SFA to measure interaction forces between silica surfaces across water, and molecular dynamics (MD) simulations of the silica–water interface to offer plausible interpretation of the experimental results. The results show that the equilibrium surface water diffusivity correlates with conventional measures of hydrophilicity (e.g., contact angle and interaction forces) and demonstrate the significance of the distribution of chemical moieties on surfaces that comprise both hydrophilic and hydrophobic chemical groups. Even though the findings are plausible after the fact, it was not clear a priori whether differences in the heterogeneity (silanol distribution) of otherwise identical silica surfaces would manifest themselves experimentally in surface water diffusivity or surface forces averaged across several water layers. While the surface chemistry of silica is still not fully understood, we propose that its tunability and the apparent effect on surface hydration thermodynamics makes it both a critical problem for understanding chemistry and processes involving silica surfaces, and a meaningful platform to study fundamental hydration phenomena.

Results and Analysis

Measurements of Silica Surface Water Diffusivity. To determine the effects of surface silanol density α_{OH} on hydration dynamics, surface water diffusivity was measured with ODNP, an NMR technique that measures the local translational water diffusivity within 1 nm of the paramagnetic spin labels in the system (30). ODNP captures equilibrium water diffusivity by single-particle dynamics by means of ^{1}H NMR relaxometry of water in the solution state. Details of the sample preparation and spin labeling procedure are given in *SI Appendix*, section S1, but briefly, we attached a stable nitroxide radical spin label [(2,2,6,6-Tetramethylpiperidin-1-yl)oxyl, TEMPO] to the surface of nonporous, fumed silica nanoparticles (Aerosil 380) at a TEMPO density of <0.03 nm^{-2} attached through an aminopropyl linkage. The particles were suspended in a 15 mM NaCl solution at pH 5.0 for ODNP measurements conducted at 22 °C.

If partially dehydroxylated silica surfaces were desired, then before the functionalization chemistry described above, the particles were heated under dry nitrogen for 6 h at temperatures ranging from 600 to 1,000 °C. The silanol density was quantified on unfunctionalized particles without TEMPO. Because partial rehydroxylation was expected during the functionalization steps in the ODNP sample preparation, the unfunctionalized particles were subjected to similar aqueous conditions before the silanol density measurement. The number of surface silanol groups per mass of silica was measured by taking the average between ^{1}H NMR measurements using deuterium exchange (5, 8) and the change in pH upon submerging the particles in a slightly basic (pH ∼9.5) solution of 1 M NaCl (10). The techniques rely on the exchangeability of the silanol protons with deuterium (from D_2O) and Na^+ (from the NaCl solution), and the results agreed well between these two complementary methods (*SI Appendix*, Table S1). The surface area per mass (specific surface area), which decreased with increased pretreatment temperature, was determined by N_2 Brunauer–Emmett–Teller (BET) measurements (31) (*SI Appendix*, Table S1).

ODNP measurements of surface water diffusivity $D_{surface}$ as a function of surface silanol density α_{OH} are shown in Fig. 1. $D_{surface}$ is particularly small, and thus the silica surfaces give rise to an unusually large retardation of surface water dynamics. Specifically, $D_{surface}$ is $(1.6–3.2) \times 10^{-10}$ m^2/s, which is ∼10× smaller than the bulk value for water (2.3×10^{-9} m^2/s) (30), ∼2–4× smaller than the value on phospholipid membranes (7.2×10^{-10} m^2/s) (32), and ∼1–5× smaller than the value on chemically heterogeneous Chemotaxis Y protein surfaces [$(2–12)\times 10^{-10}$ m^2/s)] (33). As expected, $D_{surface}$ generally decreases with increasing α_{OH} (increasing hydrophilicity), but there is a sharp decrease in $D_{surface}$ going from α_{OH} = 2.2–2.7 nm^{-2}, while $D_{surface}$ remains constant within error for α_{OH} < 2.2 and α_{OH} > 2.7 nm^{-2}. Under the same conditions as the ODNP measurements, electron paramagnetic resonance (EPR) measurements of the TEMPO-labeled silica, which give some measure of the mobility of the TEMPO moiety (32, 34), show no differences across the here-tested range of silanol densities (*SI Appendix*, Fig. S2), suggesting that the transition is not due to silica aggregation that occurs at a specific value of α_{OH}. Further, the transition does not appear to be due to a sudden change in water density near the spin labels. Electron spin echo envelope modulation (ESEEM) measurements (35) that quantify the number density of (deuterated) water in the primary hydration shell of the spin label were conducted on five of the samples, showing relatively constant water density across a range of α_{OH} (*SI Appendix*, Fig. S5). This result further suggests that the position of

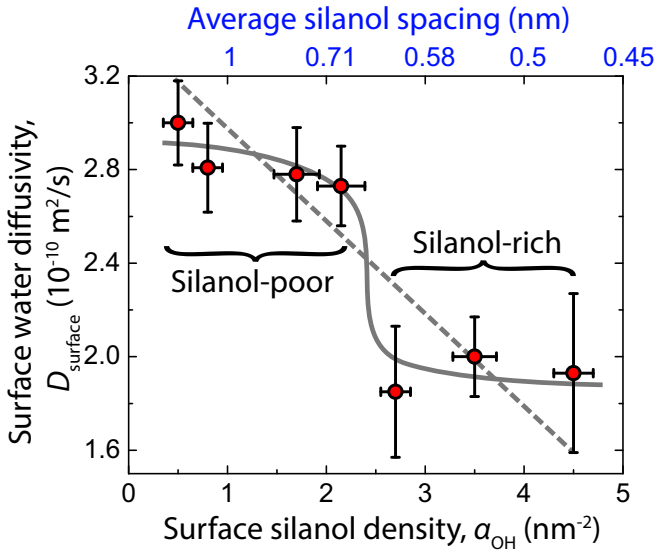

Fig. 1. Values of water diffusivity measured at the silica surface $D_{surface}$ in 15 mM NaCl, pH 5.0, and 22 °C, as measured by ODNP. Errors in $D_{surface}$ are the SD of at least three measurements at each value of α_{OH}. The surface silanol density α_{OH} was quantified by deuterium exchange and pH measurements following heat treatments at 1,000, 950, 900, 800, 700, 600, or 22 °C. There is a steep transition in $D_{surface}$ between α_{OH} = 2.2 and 2.7 nm^{-2} (corresponding to pretreatment temperatures of 800 and 700 °C, respectively). The upper *x* axis shows the average silanol spacing if one were to assume isotropically distributed silanols on the surface. The dashed gray line represents a linear trend of $D_{surface}$ with α_{OH}, which connects the extrema of the end points in the plot, but does not pass through all of the data points. The solid gray line shows the more likely trend.

the TEMPO linkage (i.e., by extension or burial) does not vary substantially across the range of α_{OH}.

Additionally, ODNP measurements on maximally hydroxylated silica (α_{OH} = 4.5 ± 0.2 nm^{-2}) were conducted at pH 3.5 and 9.0 to test the effect that deprotonated, charged silanols (SiO^-) may have on hydration dynamics, as the surface density of SiO^- groups varies by a factor of at least 50 over that pH range (36, 37). Within error, no difference was observed in the hydration dynamics [$D_{surface}$ (in units of 10^{-10} m^2/s) = 2.1 ± 0.4 at pH 3.5, 1.9 ± 0.3 at pH 5.0, and 1.8 ± 0.3 at pH 9.0]. SFA studies have also shown a minimal effect of varying surface charge density (38), as corroborated by water contact angle measurements, in which we found the contact angle to be 0° on maximally hydroxylated silica at all three pH values, suggesting that charged SiO^- groups do not contribute significantly to the observed variation in surface hydration effects. This behavior distinguishes silica from other notable surfaces on which hydration has been extensively studied, such as muscovite mica (39), acrylic polymers (40), and lipid membranes (41, 42), where surface hydration is essentially due to charged surface groups/ions with individual hydration shells and defined hydrated excluded volumes or is modulated by interactions of hydrated ions with macromolecules.

To examine the possibility of a swollen, gel-like surface layer that grows over the scale of hours–days, ODNP measurements were also performed on maximally hydroxylated silica after the particles were submerged in the 15 mM NaCl solution for 2 d. The results were unchanged after the extra immersion period [$D_{surface}$ (in units of 10^{-10} m^2/s) = 1.9 ± 0.3 initially vs. 1.8 ± 0.4 after 2 d], as was also observed in our SFA measurements on maximally hydroxylated silica surfaces (described below) and the SFA measurements of Grabbe and Horn (27) on dehydroxylated silica. The negligible contribution of silica hairs in the gel layer that would correspond to Q^1 silica is further corroborated by solid-state ^{1}H-^{29}Si cross polarization/magic-angle spinning dynamic nuclear polarization NMR (CP-MAS DNP-NMR) (*SI Appendix*, Fig. S3) that shows the Q^1 species to constitute only 1.4% of the total surface or subsurface ^{29}Si signal (*SI Appendix*, Fig. S4). The confidence in the assignment to Q^1 species can be derived from the systematic absence of this peak in freshly submerged silica, its appearance after 16 h of hydration, disappearance upon drying, and reappearance upon rehydration for an additional 16 h. Further details are in *SI Appendix*, section S2. Taken together, we can neglect the steric effect of gel-like silica species contributing to the measurement of surface hydration properties in the ODNP measurements.

Independent measurements of water contact angle, θ_o, were performed on silicon wafers pretreated in the same way as the ODNP samples shown in Fig. 1, but without using the functionalization reagents. A plot of $\cos(\theta_o)$ vs. pretreatment temperature is shown in *SI Appendix*, Fig. S6, displaying a moderately steep change between 600 and 800 °C, albeit much less dramatic than that seen in Fig. 1 between samples pretreated at 700 and 800 °C.

Force–Distance Measurements Between Silica Surfaces. To better understand how the observed trends in hydration dynamics relate to interactions between silica surfaces, the equilibrium interaction forces between silica surfaces of varying silanol density were measured with the SFA under quasi-static conditions. In the SFA experiments, the absolute distance between back-silvered silica surfaces in a cross-cylinder geometry was measured by interferometry, and the interaction force F measured by the deflection of a cantilever spring (43). The distance was controlled by moving one surface with a piezoelectric crystal in steps of 2–20 nm, and 30 s of equilibrium time was allowed before the distance was measured. Force–distance profiles are typically shown as F normalized by the radius of the surfaces R plotted against the separation distance D (i.e., F/R vs. D). Values for D = 0 correspond to silica–silica contact under dry conditions. Silica surfaces in our experiments were prepared using the "bubble method," resulting in thin (3–6 μm) sheets of glass-blown silica, described in detail elsewhere (27, 38). The silica, being mostly dehydroxylated initially (water contact angle of 38°), was subjected to UV-ozone treatments for 0.5–10 min to give water contact angles of 33°, 26°, and 0° on the surfaces. The water contact angles were used to estimate the silanol density via the Israelachvili–Gee equation (44), giving α_{OH} values of 4.6, 2.9, 2.0, and 1.2 nm^{-2}, which roughly span the range obtained in the ODNP measurements.

Representative force–distance profiles for two sets of silica surfaces are shown in Fig. 2. Decreasing the water contact angle from 33° to 26° results most notably in an added repulsion at D < 4 nm, where one would expect surface hydration to impact forces. Force profiles corresponding to θ_o = 26° match very closely with those for θ_o = 0°. The short-range repulsion decreases significantly in going from θ_o = 26° to 33°, and then remains constant up to θ_o = 38° (*SI Appendix*, Fig. S7). Force profiles were fit to the standard Derjaguin–Landau–Verwey–Overbeek (DLVO) model (45) comprising an attractive van der Waals force and a repulsive electric double-layer force (details given in *SI Appendix*, section S3). The measured forces begin to deviate from the DLVO fit below D = 4–5 nm for the 26° surface, and below D = 2–3 nm for the 33° surface. An additional short-range force that varies exponentially with distance can be added to better fit the data. The added force component increases ~2.5× in magnitude upon decreasing θ_o from 33° to 26° (see the exponential prefactor P in *SI Appendix*, Table S2).

It should also be noted that for the α_{OH} = 4.6 nm^{-2} surfaces, the forces remained unchanged after exposing the surfaces to the aqueous solution for 48 h. Furthermore, the change in silica film thickness was measured as a function of relative humidity for the most hydrophilic (α_{OH} = 4.6 nm^{-2}) and the most hydrophobic

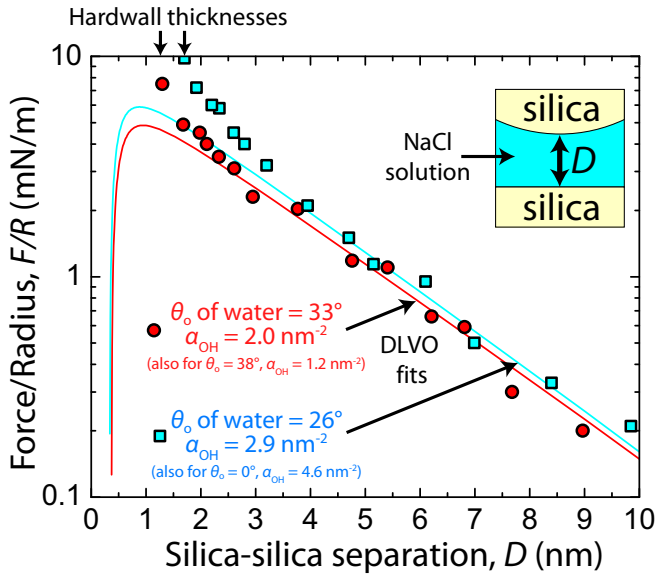

Fig. 2. Representative SFA measurements of interaction forces as a function of distance (0.1-nm distance resolution) between silica surfaces across a 15 mM NaCl solution at 22 °C. The two surfaces used in each force run displayed the same water contact angles—either θ_o = 26° or 33° (i.e., a symmetric experiment). Values of α_{OH} were calculated from the Israelachvili–Gee equation (44). The solid lines correspond to DLVO fits for each data series. A Hamaker constant A of 6.1×10^{-21} J was used (45), and fitted values for the surface potential ψ_o were −60 ± 4 mV for the 26° surface, and −55 ± 3 mV for the 33° surface. Force profiles for surfaces displaying θ_o = 0° (α_{OH} = 4.6 nm^{-2}) essentially lie on top of those for the 26° surface, and force profiles for surfaces displaying θ_o = 38° (α_{OH} = 1.2 nm^{-2}) similarly match with those for the 33° surface, so these additional profiles are omitted here for clarity, but are shown in *SI Appendix*, Fig. S7. The force measurements were conducted ∼1 h after injecting the aqueous solution between the surfaces, but measurements after 48 h showed no change for the θ_o = 0° surface.

(α_{OH} = 1.2 nm^{-2}) surfaces. Vigil et al. observed a swelling of 1.5–2.0 nm per surface (in going from 0 to 100% relative humidity) for the hydrophilic silica surfaces used in their experiments, which was partially used to justify the existence of a gelatinous layer of silica hairs that caused the short-range repulsion. Here, we observed an increase in thickness (per surface) of 0.8 nm for the α_{OH} = 4.6 nm^{-2} surface and 0.6 nm for the α_{OH} = 1.2 nm^{-2} surface in going from 0 to 100% relative humidity (*SI Appendix*, Fig. S8), which may be due to two to three layers of bound water on each surface. Based on these results, if silica hairs contributed to the short-range repulsion in the experiments of Vigil et al., they certainly contribute less in our experiments.

Simulations of the SiO_2–Water Interface. MD simulations of the SiO_2–water interface were performed to develop a molecular picture and rationale for the trends observed in Fig. 1. The simulated surface water diffusivity D_{sim} was computed for model amorphous surfaces with α_{OH} varied between 1.5 and 4.0 nm^{-2}. Methodological details related to the MD simulations and the calculation of D_{sim} are in *Materials and Methods* and *SI Appendix*, section S4. In general, values of D_{sim} were an order of magnitude larger than the ODNP $D_{surface}$ values. Both techniques probe diffusive dynamics but have conceptual differences such that one should not expect the same absolute diffusivities but rather similar qualitative trends. These differences include inaccuracy in the water model selected [the four-site transferable intermolecular potential model for Ewald techniques (TIP4P-Ew) has a slightly higher diffusivity than real water], the models used to calculate diffusivity [mean-squared displacement in simulations and the force-free hard-sphere model in ODNP (30)], and the treatment of boundary conditions in developing and applying the diffusivity models. Initial simulation results showed a near-linear trend for surface water diffusivity D_{sim} with α_{OH} (*SI Appendix*, Fig. S9). However, we found that the spatial distribution of silanols on the surface (for a given α_{OH}) could result in noticeably different D_{sim} values (i.e., the two amorphous interfaces at 4.0 nm^{-2} exhibit different D_{sim} values).

To understand the potential range of diffusivities accessible to a surface with a fixed composition (number) of silanol groups, due to their distinct possible arrangements, we used a genetic algorithm to adjust the patterning of silanol groups on crystalline cristobalite-10$\bar{1}$ surfaces to achieve maximum or minimum values of D_{sim} for four distinct α_{OH} values: 1.0, 1.5, 2.0, and 3.0 nm^{-2} (*SI Appendix*, Fig. S10). Crystalline rather than amorphous surfaces were used in the genetic algorithm optimization due to greater ease in adjusting silanol patterns without the need of adjusting the underlying surface structure (*Materials and Methods*). This choice reduces the range of D_{sim} values observed at a fixed density, as the crystalline surface intrinsically presents fewer heterogeneities in its surface structure. The results of the optimization after 70 iterations (generations), are shown in Fig. 3. The difference between maximum and minimum D_{sim} values is ∼10% for each of the four intermediate α_{OH} values (the gray area of Fig. 3*A*), but more iterations could further increase the range. The data points for α_{OH} = 0 and 4.0 nm^{-2} represent close-packed lattices of all siloxane or all silanol groups, for which no rearrangement of silanol groups is possible. Fig. 3*B* shows images of the simulated surfaces associated with the data points in Fig. 3*A*. The maximum diffusivity surfaces show a higher degree of clustering/clumping of the silanol groups than the minimum diffusivity counterparts. We quantified the clustering with an average silanol coordination number N_c, which is the average number of silanols within 5.5 Å of any given silanol. Further metrics of clustering are given in *SI Appendix*, Table S3.

Discussion and Conclusions

The ODNP and SFA measurements together reveal a significant transition in both hydration dynamics and silica–silica short-range forces between intermediate silanol densities of α_{OH} = 2.0 and 2.9 nm^{-2}, corresponding to a water contact angle of θ_o = 33° and 26°, respectively. The agreement between the ODNP and SFA results implies that the SFA-measured short-range forces comprise, to a significant degree, a hydration force in this system. The agreement further implies that the ODNP measurements were indeed probing the average hydration behavior on the surface (i.e., the spin-label distribution was uncorrelated with the surface chemical environment). Although the exact theoretical connection between hydration dynamics and surface forces is unclear (46), the agreement suggests that the equilibrium hydration dynamics as derived from ODNP can qualitatively reflect the properties of surface water that govern hydration forces on silica–water surfaces. Such connections have been previously demonstrated in the study of liposome–water surfaces by parallel SFA-ODNP measurements (42, 47).

The MD simulations show that a range of surface water diffusivities can be obtained at intermediate values of α_{OH} (1.0–2.0 nm^{-2}) through the precise patterning and spatial distribution of silanols. They also show that the connectivity of surface silanol groups has a particular impact on dynamics, with higher water diffusivity arrangements manifesting close clustering. The notion that the contribution to average surface hydration from individual surfaces groups may not be additive has precedent. By measuring water density fluctuations near a mixed self-assembled monolayer (SAM) surface by MD simulations, Acharya et al. (48) found that substituting a single hydrophilic group into a lattice of hydrophobic groups (case 1) had a far greater impact on surface hydration than the reverse substitution of a single

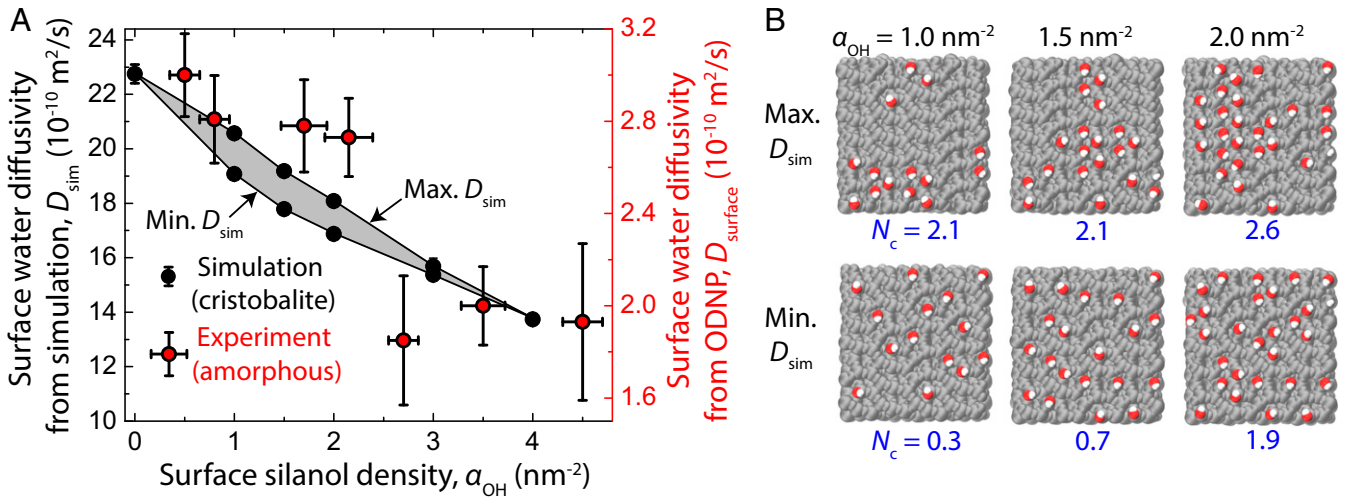

Fig. 3. MD simulations of the cristobalite–water interface. (*A*) Surface water diffusivities calculated from experiment and simulation vs. α_{OH}. The error bars for simulation are the 99% confidence interval assuming a Student's *t* distribution. The solid black lines trace out the minimum and maximum diffusivity surfaces for simulation after optimization using a genetic algorithm. (*B*) Images of the α_{OH} = 1.0, 1.5, and 2.0 nm^{-2} surfaces associated with the max and min data points in *A*. The silanol coordination number N_c associated with each surface is displayed in blue below each image.

hydrophobic group into a lattice of hydrophilic ones (case 2). Similar conclusions have been reached in other simulation studies that emphasize the importance of patterning on chemically heterogeneous surfaces (49, 50). These literature results might suggest that in Fig. 1, the slope ($D_{surface}$ vs. α_{OH}) at $\alpha_{OH} < 2.2$ nm^{-2} (similar to case 1 but without truly hydrophobic groups) should be steeper than that at $\alpha_{OH} > 2.7$ nm^{-2} (similar to case 2), but any such difference in slopes could not be observed due to the experimental uncertainty. Our simulations similarly found that the surface-projected area of the volume in which any given silanol may hydrogen bond with a water molecule decreases with increasing silanol clumping/coordination (*SI Appendix*, Table S3).

It is possible that the experimentally observed transition originates from a 2D percolation threshold, wherein all silanol groups are connected through a fluctuating but pronounced hydrogen-bond network (either silanol–silanol or silanol–water-silanol) once the clusters become large enough (51). Similar 2D percolation networks have been studied in the context of protein hydration, particularly lysozyme. Such simulations have found a critical water concentration where water forms a connected hydrogen-bond network around the curved protein surface, which is thought to correspond to sudden changes in experimentally observed physical properties such as solution capacitance, as well as the onset of some biological functions (52, 53).

It is not entirely clear whether the silica surface would become patchy during hydroxylation from a dehydroxylated state, or during dehydroxylation from a hydroxylated state. Water in the vapor phase selectively, or at least preferably, adsorbs to silanol groups (1), perhaps catalyzing hydroxylation of adjacent siloxane groups, suggesting autocatalytic growth of silanol patches during hydroxylation. If that is the case, the consistency between the ODNP and SFA results is striking given that partial rehydroxylation of the nanoparticles occurred in water, whereas rehydroxylation of the SFA surfaces occurred primarily during UV-ozone treatment (albeit under humid conditions). The consistency between ODNP and SFA is also intriguing given the difference in curvature of the silica surfaces used in the two techniques (average radii of curvature of ~3.5 nm for the nanoparticles vs. ~2 cm for the SFA surfaces). Thus, the agreement between ODNP and SFA suggests that the characteristic size of a critical cluster would potentially be no more than a few nanometers, but the fumed particles are branched and irregular, making conclusive statements difficult. Clearly, the effect of silanol distribution at intermediate silanol densities invokes robust effects on silica surface hydration that are expected to tune silica surface properties relevant to chemistry and processes involving silica surfaces.

Together, the ODNP, SFA, and MD simulation results indicate that the average surface silanol density α_{OH} alone is not sufficient to characterize the hydrophilicity of a silica surface, even if it is smooth, and further uncover the possibility that the steep change in hydration dynamics (Fig. 1) may be caused by a critical silanol cluster size or coordination number. Given the limitations of our simulations, such as the use of a model crystalline surface and the limited number of surface patterns explored (which still may not fully span the range of accessible diffusivities), the results cannot quantitatively fit those of Fig. 1. Rather, they bring to light a possible explanation for the experimental trend, and invite further investigation into the relevant metrics of silanol distributions and silanol speciation as a function of rehydroxylation procedures, as is relevant to practical applications in catalysis, geology, and nanofabrication.

Materials and Methods

Upon initial purchase of the commercial silica (Aerosil 380), the particles were heated to 85 °C in water for 1 wk to ensure maximum hydroxylation. If partially dehydroxylated silica was desired for a given experiment, ~200 mg of silica was heated in a tube furnace under dry N_2 for 6 h at the target temperature using a ramp rate of 10 °C/min. Details of the silane and spin-labeling procedures are given in *SI Appendix*, section S1. For ESEEM measurements, the 15 mM NaCl, pH 5 solution used in the ODNP measurements was replaced with a 70% D_20, 30% glycerol (vol/vol) solution in all cases, and the measurements were conducted at 80 K. Further details of the EPR and NMR measurements are in *SI Appendix*, section S2.

Nanoparticle-specific surface area was measured with the standard BET N_2 adsorption technique using a MicroMeritics TriStar 3000 Porosimeter. Silanol density was measured through deuterium exchange by immersing dry particles in D_2O containing trace (but known) amounts of HDO and 1 mM DMSO as a concentration reference. After sonicating for 10 min, the particles were removed with centrifugation (15,000 $g \times 5$ min), and the concentration of protons in the resultant liquid was quantified with ^{1}H NMR. Silanol density was also measured by immersing particles in a deaerated and slightly basic 1 M NaCl solution (pH ~ 9.5, but measured before each experiment under Ar gas), sonicating and separating out the particles as above, and measuring the pH of the resultant liquid under Ar gas. The NaCl, 3-(ethoxydimethylsilyl)propylamine (APDMES), 4-carboxy TEMPO, PBS buffer, and MES buffer reagents used were purchased from commercial suppliers and were used without further purification.

The silica SFA surfaces were prepared using the established bubble method (27, 38). Because, when using this method, the two apposing silica surfaces have different thicknesses, calculating the distance was done as in ref. 54. Water contact angle measurements were conducted using a DataPhysics OCA 25 video-based optical contact-angle measuring system. The contact angles were measured 15 s after deposition of a 2 μL droplet, and the droplet shapes were fit to a spherical cap model.

All MD simulations were carried out using the package GROMACS (release 2016.1) (55, 56). The TIP4P-Ew water model (57) was used throughout in conjunction with force-field parameters developed for crystalline and amorphous models of silica interfaces by Heinz and coworkers (58). The patterning of silanols on the surface was adjusted according to a genetic algorithm. Further details are in *SI Appendix*, section S4.

ACKNOWLEDGMENTS. We thank Susannah Scott (University of California, Santa Barbara) for insightful discussion on silica surface chemical heterogeneity. The research reported here was supported by the NSF MRSEC Program through DMR 1720256. This grant was also supported by NSF Grant CHE1505038 (to S.H.) and made use of the 9 T MAS DNP instrument acquired through NSF-MRI DMR1429710 and supported by the shared facilities of the UCSB MRSEC (NSF DMR 1720256). M.S.S. and J.I.M. also acknowledge support from the NSF (Project DMR-1312548) and a Graduate Research Fellowship (DGE 1144085).

1. Iler RK (1979) *The Chemistry of Silica* (Wiley, New York), pp 3–10, 624–648.
2. Zhuravlev LT (2000) The surface chemistry of amorphous silica. Zhuravlev model. *Colloids Surf A Physicochem Eng Asp* 173:1–38.
3. Ek S, Root A, Peussa M, Niinistö L (2001) Determination of the hydroxyl group content in silica by thermogravimetry and a comparison with 1H MAS NMR results. *Thermochim Acta* 379:201–212.
4. Gallas J-P, et al. (2009) Quantification of water and silanol species on various silicas by coupling IR spectroscopy and in-situ thermogravimetry. *Langmuir* 25:5825–5834.
5. Christy AA, Egeberg PK (2005) Quantitative determination of surface silanol groups in silicagel by deuterium exchange combined with infrared spectroscopy and chemometrics. *Analyst (Lond)* 130:738–744.
6. Ide M, et al. (2013) Quantification of silanol sites for the most common mesoporous ordered silicas and organosilicas: total versus accessible silanols. *Phys Chem Chem Phys* 15:642–650.
7. Burneau A, Barres O, Gallas J, Lavalley JC (1990) Comparative study of the surface hydroxyl groups of fumed and precipitated silicas. 2. Characterization by infrared spectroscopy of the interactions with water. *Langmuir* 6:1364–1372.
8. Hall WK, Leftin HP, Cheselske FJ, O'Reilly DE (1963) Studies of the hydrogen held by solids IV. Deuterium exchange and NMR investigations of silica, alumina, and silica-alumina catalysts. *J Catal* 2:506–517.
9. Léonardelli S, Facchini L, Fretigny C, Tougne P, Legrand AP (1992) Silicon-29 nuclear magnetic resonance study of silica. *J Am Chem Soc* 114:6412–6418.
10. Allen LH, Matijević E (1971) Stability of colloidal silica. *J Colloid Interface Sci* 35:66–76.
11. Jal PK, Patel S, Mishra BK (2004) Chemical modification of silica surface by immobilization of functional groups for extractive concentration of metal ions. *Talanta* 62:1005–1028.
12. Liu CC, Maciel GE (1996) The fumed silica surface: A study by NMR. *J Am Chem Soc* 118:5103–5119.
13. Shioji S, Hanada M, Hayashi Y, Tokami K, Yamamoto H (2007) Kinetic study of alkoxylation and rehydroxylation reactions on silica surfaces. *Adv Powder Technol* 18:467–483.
14. Young G (1958) Interaction of water vapor with silica surfaces. *J Colloid Sci* 13:67–85.
15. Sneh O, George SM (1995) Thermal stability of hydroxyl groups on a well-defined silica surface. *J Phys Chem* 99:4639–4647.
16. Wood BJ, Lamb RN, Raston CL (1995) Static SIMS study of hydroxylation of low-surface-area silica. *Surf Interface Anal* 23:680–688.
17. Chuang I-S, Maciel GE (1996) Probing hydrogen bonding and the local environment of silanols on silica surfaces via nuclear spin cross polarization dynamics. *J Am Chem Soc* 118:401–406.
18. Perras FA, Chaudhary U, Slowing II, Pruski M (2016) Probing surface hydrogen bonding and dynamics by natural abundance, multidimensional, 17O DNP-NMR spectroscopy. *J Phys Chem C* 120:11535–11544.
19. Fleischman SD, Scott SL (2011) Evidence for the pairwise disposition of grafting sites on highly dehydroxylated silicas via their reactions with Ga(CH3)3. *J Am Chem Soc* 133:4847–4855.
20. Ugliengo P, et al. (2008) Realistic models of hydroxylated amorphous silica surfaces and MCM- 41 mesoporous material simulated by large-scale periodic B3LYP calculations. *Adv Mater* 20:4579–4583.
21. Ewing CS, Bhavsar S, Veser G, McCarthy JJ, Johnson JK (2014) Accurate amorphous silica surface models from first-principles thermodynamics of surface dehydroxylation. *Langmuir* 30:5133–5141.
22. Gallo P, Rovere M, Chen S-H (2010) Anomalous dynamics of water confined in MCM-41 at different hydrations. *J Phys Condens Matter* 22:284102.
23. Bourg IC, Steefel CI (2012) Molecular dynamics simulations of water structure and diffusion in silica nanopores. *J Phys Chem C* 116:11556–11564.
24. West R, Whatley LS, Lake KJ (1961) Hydrogen bonding studies. V. The relative basicities of ethers, alkoxysilanes and siloxanes and the nature of the silicon-oxygen bond. *J Am Chem Soc* 83:761–764.
25. Lamb RN, Furlong DN (1982) Controlled wettability of quartz surfaces. *J Chem Soc Faraday Trans 1* 78:61–73.
26. Vigil G, Xu Z, Steinberg S, Israelachvili J (1994) Interactions of silica surfaces. *J Colloid Interface Sci* 165:367–385.
27. Grabbe A, Horn R (1993) Double-layer and hydration forces measured between silica sheets subjected to various surface treatments. *J Colloid Interface Sci* 157:375–383.
28. Chapel JP (1994) Electrolyte species dependent hydration forces between silica surfaces. *Langmuir* 10:4237–4243.
29. Grabbe A (1993) Double layer interactions between silylated silica surfaces. *Langmuir* 9:797–801.
30. Franck JM, Pavlova A, Scott JA, Han S (2013) Quantitative cw Overhauser effect dynamic nuclear polarization for the analysis of local water dynamics. *Prog Nucl Magn Reson Spectrosc* 74:33–56.
31. Brunauer S, Emmett PH, Teller E (1938) Adsorption of gases in multimolecular layers. *J Am Chem Soc* 60:309–319.
32. Cheng CY, Song J, Pas J, Meijer LH, Han S (2015) DMSO induces dehydration near lipid membrane surfaces. *Biophys J* 109:330–339.
33. Barnes R, et al. (2017) Spatially heterogeneous surface water diffusivity around structured protein surfaces at equilibrium. *J Am Chem Soc* 139:17890–17901.
34. Columbus L, Hubbell WL (2002) A new spin on protein dynamics. *Trends Biochem Sci* 27:288–295.
35. Schweiger A, Jeschke G (2001) *Principles of Pulsed Electron Paramagnetic Resonance* (Oxford Univ Press, New York).
36. Behrens SH, Grier DG (2001) The charge of glass and silica surfaces. *J Chem Phys* 115:6716–6721.
37. Kobayashi M, Skarba M, Galletto P, Cakara D, Borkovec M (2005) Effects of heat treatment on the aggregation and charging of Stöber-type silica. *J Colloid Interface Sci* 292:139–147.
38. Horn R, Smith D, Haller W (1989) Surface forces and viscosity of water measured between silica sheets. *Chem Phys Lett* 162:404–408.
39. Pashley RM (1981) Forces between mica surfaces in Li^+, Na^+, K^+, and Cs^+ electrolyte solutions: A correlation of double-layer and hydration forces with surface cation exchange. *J Colloid Interface Sci* 83:531–546.
40. Zhang Y, Cremer PS (2006) Interactions between macromolecules and ions: The Hofmeister series. *Curr Opin Chem Biol* 10:658–663.
41. Marra J, Israelachvili J (1985) Direct measurements of forces between phosphatidylcholine and phosphatidylethanolamine bilayers in aqueous electrolyte solutions. *Biochemistry* 24:4608–4618.
42. Schrader AM, et al. (2015) Correlating steric hydration forces with water dynamics through surface force and diffusion NMR measurements in a lipid-DMSO-H_2O system. *Proc Natl Acad Sci USA* 112:10708–10713.
43. Israelachvili JN, et al. (2010) Recent advances in the surface forces apparatus (SFA) technique. *Rep Prog Phys* 73:1–16.
44. Israelachvili J, Gee M (1989) Contact angles on chemically heterogeneous surfaces. *Langmuir* 2:288–289.
45. Israelachvili JN (2011) *Intermolecular and Surface Forces* (Elsevier, San Diego), 3rd Ed, pp 254–267, 312–332.
46. Luzar A, Chandler D (1996) Hydrogen-bond kinetics in liquid water. *Nature* 379:55–57.
47. Schrader AM, Cheng CY, Israelachvili JN, Han S (2016) Communication: Contrasting effects of glycerol and DMSO on lipid membrane surface hydration dynamics and forces. *J Chem Phys* 145:041101.
48. Acharya H, Vembanur S, Jamadagni SN, Garde S (2010) Mapping hydrophobicity at the nanoscale: applications to heterogeneous surfaces and proteins. *Faraday Discuss* 146:353–365, discussion 367–393, 395–401.
49. Giovambattista N, Debenedetti PG, Rossky PJ (2007) Hydration behavior under confinement by nanoscale surfaces with patterned hydrophobicity and hydrophilicity. *J Phys Chem C* 111:1323–1332.
50. Giovambattista N, Debenedetti PG, Rossky PJ (2009) Enhanced surface hydrophobicity by coupling of surface polarity and topography. *Proc Natl Acad Sci USA* 106:15181–15185.
51. Hoshen J, Kopelman R (1976) Percolation and cluster distribution. I. Cluster multiple labeling technique and critical concentration algorithm. *Phys Rev B* 14:3438–3445.
52. Oleinikova A, Smolin N, Brovchenko I, Geiger A, Winter R (2005) Formation of spanning water networks on protein surfaces via 2D percolation transition. *J Phys Chem B* 109:1988–1998.
53. Careri G, Giansanti A, Rupley JA (1986) Proton percolation on hydrated lysozyme powders. *Proc Natl Acad Sci USA* 83:6810–6814.
54. Horn RG, Smith DT (1991) Analytic solution for the three-layer multiple beam interferometer. *Appl Opt* 30:59–65.
55. Abraham MJ, et al. (2015) Gromacs: High performance molecular simulations through multi-level parallelism from laptops to supercomputers. *SoftwareX* 1–2:19–25.
56. Szilárd P, Abraham MJ, Kutzner C, Hess B, Lindahl E (2015) Tackling exascale software challenges in molecular dynamics simulations with GROMACS. *Lect Notes Comput Sci* 8759:3–27.
57. Horn HW, et al. (2004) Development of an improved four-site water model for biomolecular simulations: TIP4P-Ew. *J Chem Phys* 120:9665–9678.
58. Emami FS, et al. (2014) Force field and a surface model database for silica to simulate interfacial properties in atomic resolution. *Chem Mater* 26:2647–2658.